Squeezed-input, optical-spring, signal-recycled gravitational-wave detectors

Jan Harms,[1] Yanbei Chen,[2] Simon Chelkowski,[1] Alexander Franzen,[1] Henning Vahlbruch,[1] Karsten Danzmann,[1] and Roman Schnabel[1]

[1]*Institut für Atom- und Molekülphysik, Universität Hannover and Max-Planck-Institut für Gravitationsphysik (Albert-Einstein-Institut), Callinstr. 38, 30167 Hannover, Germany*

[2]*Theoretical Astrophysics 130-33, California Institute of Technology, Pasadena, California 91125, USA*

(Received 26 March 2003; published 21 August 2003)

We theoretically analyze the quantum noise of signal-recycled laser interferometric gravitational-wave detectors with additional input and output optics, namely, frequency-dependent squeezing of the vacuum state of light entering the dark port and frequency-dependent homodyne detection. We combine the work of Buonanno and Chen on the quantum noise of signal-recycled interferometers with ordinary input and output optics, and the work of Kimble *et al.* on frequency-dependent input and output optics with conventional interferometers. Analytical formulas for the optimal input and output frequency dependencies are obtained. It is shown that injecting squeezed light with the optimal frequency-dependent squeezing angle into the dark port yields an improvement in the noise spectral density by a factor of e^{-2r} (in power) over the entire squeezing bandwidth, where r is the squeezing parameter. It is further shown that a frequency-dependent (variational) homodyne readout leads to an additional increase in sensitivity which is significant in the wings of the doubly resonant structure. The optimal variational input squeezing in the case of an ordinary output homodyne detection is shown to be realizable by applying two optical filters on a frequency-independent squeezed vacuum. Throughout this paper, we take as an example the signal-recycled topology currently being completed at the GEO 600 site. However, theoretical results obtained here are also applicable to the proposed topology of the Advanced LIGO.

DOI: 10.1103/PhysRevD.68.042001 PACS number(s): 04.80.Nn, 03.65.Ta, 42.50.Dv, 95.55.Ym

I. INTRODUCTION

Gravitational waves (GWs) were predicted long ago by Einstein using the theory of general relativity, but so far have not been directly observed [1]. Currently, an international array of first-generation, kilometer-scale laser interferometric gravitational-wave detectors, consisting of GEO 600 [2], The Laser Interferometer Gravitational-wave Observatory (LIGO) [3], TAMA 300 [4], and VIRGO [5], targeted at gravitational waves in the acoustic band from 10 Hz to 10 kHz, is going into operation. These first-generation detectors are all Michelson interferometers with suspended mirrors. Injecting a strong carrier light from the bright port, the antisymmetric mode of arm-length oscillations (e.g., excited by a gravitational wave) yields a sideband modulation field in the antisymmetric (optical) mode which is detected at the dark output port. To yield a high sensitivity to gravitational waves, long arm lengths of 300 m up to 4 km and circulating laser power on the order of 10 kW are going to be realized in 2003 with the help of the technique of *power recycling* [6].

GEO 600 is the only first-generation detector that not only uses power recycling, but also includes the more advanced technique of *signal recycling* [7]. The idea of signal recycling is to retroreflect part of the signal light at the dark port back into the interferometer, establishing an additional cavity which can be set to resonate at a desired gravitational-wave frequency. Signal recycling leads to a well known (optical) resonance structure in the interferometer's noise curve. This resonance can already beat the standard quantum limit (SQL) [8,9], which is the lower bound for the noise of conventional interferometers without signal recycling and with conventional input and output optics. A further benefit of signal recycling is the reduced optical loss due to imperfect mode matching from the *mode healing effect* [10]. The next-generation detectors currently being planned are likely to use this technique, for example are Advanced LIGO (also known as LIGO-II) [11].

Buonanno and Chen also predict a second, optomechanical resonance in signal-recycled interferometers, around which the interferometer gains sensitivity and can also beat the standard quantum limit [8,9,12,13]. The work of Buonanno and Chen has been limited to signal-recycled interferometers with arm cavities, or interferometers with a single end mirror in each arm, and with infinitely heavy beam splitters. In all cases considered, coherent vacuum was entering the interferometer's dark port, i.e., no additional input and output optics were investigated. On the other hand, Kimble *et al.* investigated these additional input and output optics for the conventional LIGO detector topology without signal recycling [14], building on earlier work treating squeezed-input interferometers [15–19] and variational-output interferometers [20–24].

In this paper, we investigate (i) the benefit of injecting squeezed vacuum with frequency-dependent squeezing angle into the interferometer's dark port and (ii) the benefit of frequency-dependent (variational) homodyne readout. We use the two-photon input-output formalism of quantum optics [25] which was also used by Kimble *et al.* and Buonanno and Chen. In Secs. III and IV of this paper, analytical expressions for the optimal frequency dependencies of the squeezing angle and homodyning angle for optical-spring signal-recycled interferometers are derived. We present our results in terms of quantum noise spectral densities. Using the Michelson topology of GEO 600 as an example for a signal-

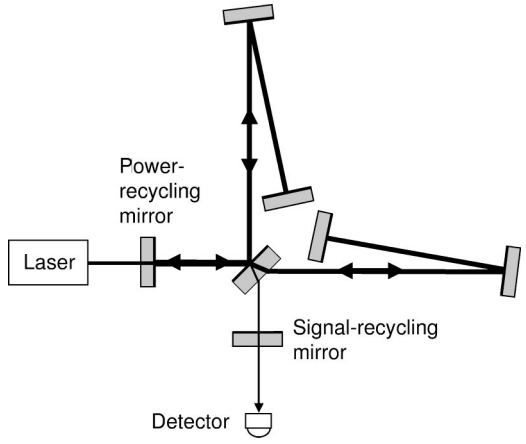

FIG. 1. GEO 600 is a dual-recycled Michelson interferometer with a power-recycling mirror in the bright port that enhances the light power within the Michelson arms and a signal-recycling mirror in the dark port that can be tuned on a specific signal frequency. Since the arms are folded once, the effective arm length is doubled to 1200 m.

recycled interferometer, quantum noise spectral densities without and with additional input and output optics are plotted and compared. Unlike the LIGO, VIRGO, and TAMA 300 interferometers, GEO 600 has folded arms and no arm cavities (Fig. 1). As we will explain, the folded-arm Michelson topology of GEO 600 has a very similar input-output relation to that of a signal-recycled Michelson interferometer topology with arm cavities. Consequently, results from this paper will also be readily applicable to the Advanced LIGO topology.

II. SIGNAL RECYCLING

In the signal-recycling optical topology, a so-called signal-recycling mirror is put into the dark port of a Michelson interferometer. This signal-recycling mirror forms a cavity, the signal-recycling cavity, with the two end mirrors of the interferometer (see Fig. 1). The length of the signal-recycling cavity can be tuned independently and can be made resonant at some signal frequency Ω. In this way, the signal is recycled and amplified due to an increased interaction time. The original idea of signal recycling SR was due to Meers [7], who proposed its use for *dual recycling*, which is the combination of power and signal recycling. Later, Mizuno *et al.* [26,27] proposed the scheme of *resonant sideband extraction*, which uses a detuned signal-recycling mirror to extract the signal from high-finesse arm cavities. Both schemes of detuned signal-recycling cavities have been experimentally demonstrated by Heinzel *et al.* [28–30] and Freise *et al.* [31] with the 30 m laser interferometer in Garching near Munich. Since GEO 600 has no arm cavities (Fig. 1), the SR mirror will have to be operated close to resonance with the carrier frequency in order to gain sensitivity comparable to that of configurations with arm cavities. Recently, the GEO 600 interferometer in Ruthe near Hannover was completed by the implementation of a signal-recycling mirror SRM. Relevant technical parameters of GEO 600 are summarized in Table I.

TABLE I. Technical data and parameter values of GEO 600 which were used to calculate the noise spectral densities in Figs. 2–4 below.

Symbol	Physical meaning	Numerical value
m	Mirror mass (each)	5.6 kg
L	Effective arm length	1200 m
P	Circulating light power	10 kW
ω_0	Angular frequency of carrier light	1.77×10^{15} s^{-1}
ρ	Power reflectivity of SRM	0.99
ϕ	SR cavity detuning	0.0055 rad

Whereas it was well known that signal-recycled interferometers exhibit an optical resonance, Buonanno and Chen [8,9] have recently shown that SR interferometers exhibit a second resonance, which is optomechanical. This resonance stems from the classical optomechanical coupling of the light field with the antisymmetric mode of the otherwise free mirrors [12]: in detuned signal-recycling schemes, the phase-modulation sidebands induced by a gravitational wave are partly converted into amplitude modulations, which beat with the carrier field, producing a motion-dependent force and acting back on the test masses.

This classical back-action force can be thought of as generated by an *optical spring*. Because of the optical spring, the test masses are no longer free — their resonant frequencies can get shifted upward into the detection band. The interferometer gains sensitivity on and around this resonance and can beat the standard quantum limit [8,9,12]. Whereas the optical resonance is primarily determined by the detuning of the SR cavity with respect to the carrier frequency ω_0 (Fig. 5.8 in [32]), the optomechanical resonance appears at a spe-

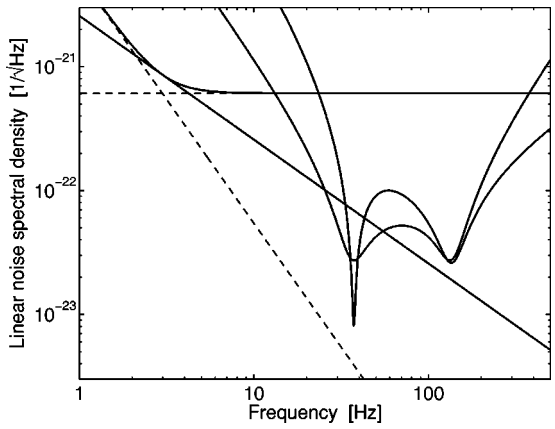

FIG. 2. The dashed lines represent the uncorrelated white shot noise and the radiation-pressure noise (proportional to f^{-2}). The sum of these shot and radiation-pressure noises yields the noise spectral density of a simple Michelson interferometer without arm cavities, here using GEO 600 parameters and $\rho=0$ (and detecting the output phase quadrature). This noise curve is limited by the SQL, which is shown as the straight solid curve. In comparison, the noise spectral densities of both orthogonal quadratures of the signal-recycled GEO 600 output field exhibit a doubly resonant structure that beats the SQL.

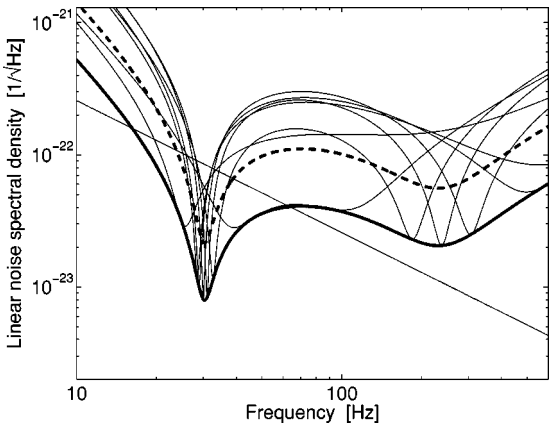

FIG. 3. The bold dashed curve shows the phase quadrature noise spectral density of a SR interferometer with unsqueezed (coherent) vacuum input. The array of thin black curves evolves from the dashed curve, if the input vacuum field at the dark port is squeezed with squeezing parameter $r=1$ and the squeezing angle λ is varied in a frequency-independent manner. The array is bounded from below by the lower bold black curve. Alternatively, one obtains the lower boundary if the conventional SR noise spectral density is simply shifted downward by a factor of e^{-r}. The same holds for the amplitude quadrature. The straight line represents the standard quantum limit.

cific sideband frequency of the carrier light which depends on the interferometer's topology, the mirror masses m, the light power P inside the interferometer, and the detuning ϕ of the SR cavity from its resonance. The optomechanical coupling of the light field with the antisymmetric mode of the interferometer also leads to the phenomenon of ponderomotive squeezing [33], i.e., the amplitude and phase quantum noise become correlated. This quantum effect is automatically considered by the formalism revealing the optical-spring behavior. However, as pointed out in [9], in SR interferometers the ponderomotive squeezing seems to be only a secondary factor that enables the interferometer to beat the SQL, whereas the *classical* resonant amplification of the signal provides the main factor.

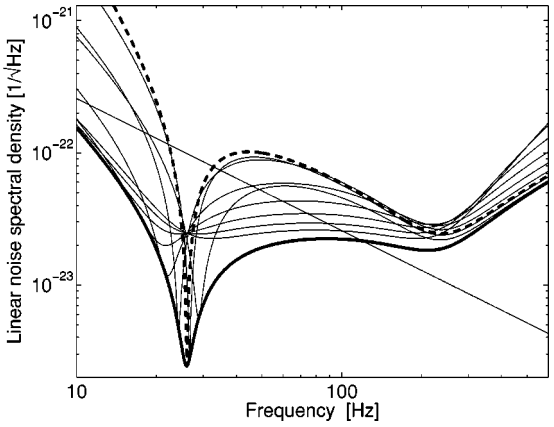

FIG. 4. Another improvement of the noise spectral densities in SR interferometers is achieved when the detection angle is optimized for each signal frequency. Since the shot noise and radiation-pressure noise are highly correlated, especially in the detection band, the effect is less beneficial than the optimization of the input squeezing angle. However, comparing the boundary curve with the dashed curve which corresponds to an arbitrary but fixed detection angle, the bandwidth of the noise minima is enhanced and a noise reduction by a factor of 10 can be achieved at some frequencies.

The investigations led by Buonanno and Chen focused on the topology of the proposed Advanced LIGO configuration, which consists of a dual-recycled Michelson interferometer with a Fabry-Pérot cavity in each arm. Due to the weak light power (compared to power in the arms) at the beam splitter, the optomechanical coupling of the light with the beam splitter's motion was neglected. In contrast, GEO 600 is a dual-recycled interferometer that builds up a high-intensity field by means of a power-recycling mirror in the bright port of the interferometer. Therefore, the motion of the beam splitter in GEO 600 is affected by power fluctuations of fields impinging from different directions. Nevertheless, assuming that the laser is shot-noise limited, the optomechanical coupling at the beam splitter exerts only minor changes on the noise spectrum of the output. It can intuitively be understood that the quantum back-action noise associated with the arm mirrors, which have a reduced mass of 1/5 the actual mirror mass due to folding the arms, clearly dominates the beam splitter of $m_{\mathrm{BS}}=9.3$ kg. Throughout this paper we do not consider the effect of radiation-pressure noise on the beam splitter. This has also been studied but will be presented in detail elsewhere [34]. Henceforth, the term ''ideal GEO 600'' refers to the interferometer in which the optomechanical coupling of the beam splitter is neglected.

The optical noise in an interferometer can be expressed in terms of the (single-sided) noise spectral density S_h of the output field normalized by the transfer function of the signal. The noise spectral density is obtained from the *input-output relation*, which maps the numerous input fields $\mathbf{i}_n$ and the gravitational-wave signal $h=\Delta L/L$ onto the detected output field $\bar{\mathbf{o}}$. Here we note that no additional noise due to the quantization of the test masses has to be considered. The sole forms of quantum noise affecting the output noise in interferometric gravitational wave detectors are the shot noise and the radiation-pressure noise [35].

The following calculations are most easily accomplished in the Caves-Schumaker two-photon formalism [25], where the optical fields are decomposed into amplitude and phase quadratures, which can then be put together into a vector, e.g., for the output field of the interferometer

$$\bar{\mathbf{o}}=\begin{pmatrix}\hat{o}_1\\ \hat{o}_2\end{pmatrix}, \tag{1}$$

where $\hat{o}_{1,2}$ are the output amplitude and phase quadratures. The input-output relation for a lossless SR interferometer can be cast into the following form:

$$\bar{\mathbf{o}}=\frac{1}{M}[\mathbf{T}\bar{\mathbf{i}}+\bar{\mathbf{s}}\ h], \tag{2}$$

TABLE II. Definitions of $\mathcal{K}$ (see [41]), h_{SQL}, and Φ for GEO 600 and Advanced LIGO topologies. Here m is the individual mirror mass, L the Michelson arm length, P the input power at the beam splitter, ω_0 the laser angular frequency, $\gamma_{\mathrm{arm}}=\tau_{\mathrm{arm}}^2 c/(4L)$ the half linewidth of the Advanced LIGO arm cavity (where τ_{arm} is the input test-mass mirror amplitude transmissivity), and Ω the GW sideband angular frequency. Values for Advanced LIGO are kept to the leading order of τ_{arm}^2, as in Refs. [8,9,12].

Symbol	GEO 600	Advanced LIGO
$\mathcal{K}$	$\dfrac{20P\omega_0}{mc^2\Omega^2}$	$\dfrac{8P\omega_0}{mL^2\Omega^2(\Omega^2+\gamma_{\mathrm{arm}}^2)}$
h_{SQL}	$\dfrac{20\hbar}{m\Omega^2L^2}$	$\dfrac{8\hbar}{m\Omega^2L^2}$
Φ	$\dfrac{\Omega L}{c}$	$\arctan\left[\dfrac{\Omega}{\gamma_{\mathrm{arm}}}\right]$

where $\bar{\mathbf{i}}$ denotes the vacuum field entering the interferometer from the dark port. The four components of the 2×2 transfer matrix $\mathbf{T}$ are given by [32]

$$T_{11,22}=e^{2i\Phi}\left[(1+\rho^2)\left(\cos(2\phi)+\frac{\mathcal{K}}{2}\sin(2\phi)\right)-2\rho\cos(2\Phi)\right],$$

$$T_{12}=-e^{2i\Phi}\tau^2[\sin(2\phi)+\mathcal{K}\sin^2(\phi)], \tag{3}$$

$$T_{21}=e^{2i\Phi}\tau^2[\sin(2\phi)-\mathcal{K}\cos^2(\phi)],$$

and M is given by

$$M=1+\rho^2e^{4i\Phi}-2\rho e^{2i\Phi}\left(\cos(2\phi)+\frac{\mathcal{K}}{2}\sin(2\phi)\right). \tag{4}$$

Thus, $\mathbf{T}$ contains an overall phase factor $e^{2i\Phi}$. ρ and τ denote the amplitude reflectivity and transmissivity of the SR mirror. The signal transfer functions $\bar{\mathbf{s}}$ for the two quadratures are given by

$$\hat{s}_1=-\frac{\sqrt{2\mathcal{K}}}{h_{\mathrm{SQL}}}\ \tau\ (1+\rho\,e^{2i\Phi})\sin(\phi),$$

$$\hat{s}_2=-\frac{\sqrt{2\mathcal{K}}}{h_{\mathrm{SQL}}}\ \tau\ (-1+\rho\,e^{2i\Phi})\cos(\phi). \tag{5}$$

Remarkably, the input-output relations are formally identical for both configurations, Advanced LIGO and ideal GEO600. Their distinguishing properties lie in the definition of the optomechanical coupling constant $\mathcal{K}$, the standard quantum limit h_{SQL}, and the phase angle Φ, which are also functions of the gravitational-wave-induced modulation frequency Ω, as listed in Table II. A phase-sensitive measurement (i.e., homodyne or heterodyne) yields a photocurrent that depends linearly on a certain combination of the two output quadrature fields:

$$\hat{o}_\zeta=\hat{o}_1\cos\zeta+\hat{o}_2\sin\zeta, \tag{6}$$

where ζ is the homodyne angle (i.e., the angle of homodyne detection). The radiation-pressure forces acting on the mirrors are proportional to the amplitude quadrature, and the motion-induced sideband fields are excitations of the light's phase quadrature. The noise spectral density S_h when detecting the quadrature $\hat{o}_\zeta$ is determined by the transfer matrix $\mathbf{T}$ and the signal transfer functions $\bar{\mathbf{s}}$. It assumes the form (see, e.g., Ref. [8])

$$S_h=\frac{(\cos\zeta\ \ \sin\zeta)\mathbf{T}\mathbf{T}^\dagger\begin{pmatrix}\cos\zeta\\ \sin\zeta\end{pmatrix}}{(\cos\zeta\ \ \sin\zeta)\bar{\mathbf{s}}\,\bar{\mathbf{s}}^\dagger\begin{pmatrix}\cos\zeta\\ \sin\zeta\end{pmatrix}}, \tag{7}$$

provided that the input field $\bar{\mathbf{i}}$ entering from the dark port is a coherent vacuum field. If $\bar{\mathbf{s}}$ is a complex vector, the product $\bar{\mathbf{s}}\,\bar{\mathbf{s}}^\dagger$ has to be replaced by the symmetrized product

$$\langle\bar{\mathbf{s}}\,\bar{\mathbf{s}}^\dagger\rangle_{\mathrm{sym}}=\frac{1}{2}(\bar{\mathbf{s}}\,\bar{\mathbf{s}}^\dagger+\bar{\mathbf{s}}^*\bar{\mathbf{s}}^{\mathrm{T}}). \tag{8}$$

The same holds for the matrix product $\mathbf{T}\mathbf{T}^\dagger$ in the numerator. Its symmetrization becomes necessary if a more general interferometer topology is considered with complex coupling constant $\mathcal{K}$. The expression in Eq. (7) for the noise spectral density is valid for any optical system whose transfer function can be given in the form of Eq. (2).

Using Eq. (7) and the parameters and definitions in Tables I and II, we are now able to plot the square root of the noise spectral density (linear noise spectral density) of the ideal GEO 600 topology for output quadrature fields of arbitrary values of the angle ζ.

Figure 2 shows the spectral densities $\sqrt{S_h(\zeta=0)}$ and $\sqrt{S_h(\zeta=\pi/2)}$ as functions of frequency, in comparison with the SQL (straight solid line). It can be seen that for both quadrature angles the SQL is beaten at frequencies around 30 Hz. This noise minimum is due to the optomechanical resonance (i.e., the optical-spring effect) and is more significant for the phase quadrature case ($\zeta=\pi/2$). The second minimum at around 200 Hz corresponds to the optical resonance of the SR cavity. This resonance can also beat the SQL when higher reflectivities of the SR mirror ρ are used. For further comparison, the quantum noise limit of a conventional GEO 600 without signal recycling is also given (solid line in the upper part of Fig. 2). The dashed lines represent the two contributions to this (conventional) limit, the uncorrelated white shot noise and the radiation-pressure noise (proportional to f^{-2}). The limit given here is calculated for a circulating light power of $P=10$ kW that reaches the SQL at 3 Hz and of course can never beat the SQL. It is interesting to note that light powers of around 1 MW are needed to shift

the conventional limit downwards to get standard quantum-noise-limited sensitivity at around 100 Hz (not shown in Fig. 2).

In the next two sections we investigate how the sub-SQL noise spectral densities of signal-recycled gravitational-wave detectors can be further improved by squeezed light injected into the dark port of the interferometer and by a frequency-dependent readout scheme.

III. SIGNAL RECYCLING AND SQUEEZED-LIGHT INPUT

As first proposed by Caves [15], squeezed light can be employed to reduce the high power requirements in GW interferometers. Later, Unruh [16] and others [14,17–19] found and proved in different ways that squeezed light with a frequency-dependent orientation of the squeezing ellipse can reduce the quantum noise down to values below the standard quantum limit. This research was done on interferometer topologies without signal recycling. Chickarmane *et al.* [36,37] investigated the squeezed-input signal-recycled interferometer at low laser powers, i.e., the shot-noise limited case. In this section we consider the squeezed-input signal-recycled interferometer at high laser powers, including the effect of back-action noise.

As discussed in Sec. IV B of Ref. [14], the squeezed vacuum is related to the ordinary coherent vacuum state by a unitary operator

$$|\mathrm{in}\rangle = S(r,\lambda)|0\rangle, \tag{9}$$

where r is the squeezing parameter and λ the squeezing angle (for an introduction to squeezed light, see, for example, [38]). Alternatively, we can transform the input state back to the vacuum state, by

$$|\mathrm{in}\rangle \rightarrow S^{\dagger}(r,\lambda)|\mathrm{in}\rangle = |0\rangle, \tag{10}$$

and at the same time transform the input quadrature operators accordingly [Eq. (A8) of Ref. [14]],

$$\begin{aligned}\bar{\mathbf{i}} &\rightarrow S^{\dagger}(r,\lambda)\bar{\mathbf{i}}S(r,\lambda)\\ &= \mathcal{D}(-\lambda)\mathcal{S}(r)\mathcal{D}(\lambda)\bar{\mathbf{i}},\end{aligned} \tag{11}$$

where

$$\mathcal{D}(\lambda) \equiv \begin{pmatrix} \cos\lambda & \sin\lambda \\ -\sin\lambda & \cos\lambda \end{pmatrix}, \quad \mathcal{S}(r) \equiv \begin{pmatrix} e^{r} & 0 \\ 0 & e^{-r} \end{pmatrix}. \tag{12}$$

From Eq. (11), we also see that a squeezed vacuum with squeezing angle λ can be obtained from a second quadrature squeezing by applying a rotation of $\mathcal{D}(-\lambda)$ (note the minus sign). Any further rotation of quadratures will also add (with a minus sign) to the squeezing angle.

The input-output relation of the lossless interferometer with fixed beam splitter becomes

$$\bar{\mathbf{o}} = \frac{1}{M}[\mathbf{T}\mathcal{D}(-\lambda)\mathcal{S}(r)\mathcal{D}(\lambda)\bar{\mathbf{i}} + \bar{\mathbf{s}}h], \tag{13}$$

implying a noise spectral density of

$$S_h = \frac{(\cos\zeta \quad \sin\zeta)\mathbf{T}\mathcal{D}(-\lambda)\mathcal{S}(2r)\mathcal{D}(\lambda)\mathbf{T}^{\dagger}\begin{pmatrix}\cos\zeta\\ \sin\zeta\end{pmatrix}}{(\cos\zeta \quad \sin\zeta)\overline{\mathbf{s}\mathbf{s}^{\dagger}}\begin{pmatrix}\cos\zeta\\ \sin\zeta\end{pmatrix}}. \tag{14}$$

Note that here $\mathbf{T}$ is a real matrix with an overall phase factor in front [cf. Eq. (3)]. Figure 3 shows an array consisting of seven curves (thin lines) where the quadrature angle $\zeta = \pi/2$ is constant and the frequency-independent squeezing angle λ is varied from 0 to 3 in equidistant steps. In all cases the squeezing parameter r has been set to unity. Interestingly, a variation of the frequency-independent squeezing angle causes a frequency shift of both resonances. For comparison, the standard quantum limit (straight line) and the noise spectral density in the quadrature at $\zeta = \pi/2$ without squeezed input (dashed line) are also given. As we can see, each individual frequency-independent value for λ can be advantageous to the case without squeezing only in a certain frequency band. Obviously, the envelope of the minima of the squeezed-input array, as also drawn in the graph (lower bold line), is physically meaningful since it can in principle be realized by applying squeezed light with a squeezing angle optimized for each sideband frequency. Such light is called frequency-dependent squeezed light and yields a broadband improvement in the quantum-noise limited sensitivity. In the final paragraphs of this section we now derive an analytical expression for the optimized noise spectral density. Suppose now the squeezing angle λ can be an arbitrary function of frequency, and r is always positive, then as we can tell from Eq. (14), the optimal $\lambda(\Omega)$ should make

$$\mathcal{D}(\lambda(\Omega))\mathbf{T}^{\dagger}\begin{pmatrix}\cos\zeta\\ \sin\zeta\end{pmatrix} \propto \begin{pmatrix}0\\ 1\end{pmatrix} \tag{15}$$

or

$$\tan\lambda(\Omega) = -\frac{T_{11}\cos\zeta + T_{21}\sin\zeta}{T_{12}\cos\zeta + T_{22}\sin\zeta}, \tag{16}$$

yielding an optimal noise spectrum of

$$S_h^{\mathrm{SI}} = e^{-2r}\frac{(\cos\zeta\,\sin\zeta)\mathbf{T}\mathbf{T}^{\dagger}\begin{pmatrix}\cos\zeta\\ \sin\zeta\end{pmatrix}}{(\cos\zeta\,\sin\zeta)\overline{\mathbf{s}\mathbf{s}^{\dagger}}\begin{pmatrix}\cos\zeta\\ \sin\zeta\end{pmatrix}}. \tag{17}$$

This expression turns out to be identical to the noise spectral density without squeezing in Eq. (7) being suppressed by a factor of e^{-2r}. This result can be understood intuitively as follows. The input quadrature field is going to be rotated (and possibly ponderomotively squeezed) by the matrix $\mathbf{T}$ before being detected. The minimal noise quadrature of the squeezed state should therefore be rotated conversely before being injected into the interferometer, such that the detector always ''sees'' the minimal noise.

A squeezed vacuum can be generated with a variable but frequency-independent squeezing angle λ (see, for example,

[39]). A frequency-dependent squeezing angle can be obtained subsequently by filtering the initial squeezed light through detuned Fabry-Perot (FP) cavities, as proposed by Kimble *et al.* [14], which can rotate the quadratures in a frequency-dependent way. For small frequencies ($\Omega \ll c/L_{\rm FP}$), a detuned FP cavity of length $L_{\rm FP}$ rotates the reflected quadrature in the following way:

$$\bar{\mathbf{a}}^{\rm out} = e^{i\alpha_{\rm m}} \mathcal{D}(-\alpha_p)\bar{\mathbf{a}}^{\rm in} \tag{18}$$

with

$$\alpha_{p,m} = \frac{1}{2}(\alpha_+ \pm \alpha_-) \tag{19}$$

and

$$\alpha_\pm = 2\ \arctan(\xi \pm \Omega/\delta). \tag{20}$$

where ξ is defined by the resonant frequency $\omega_{\rm FP}$ and by δ, which is the half linewidth of the cavity: $\omega_{\rm FP} = \omega_0 - \xi\delta$. As further shown by Purdue and Chen in Appendix A of Ref. [40], several such Fabry-Perot filter cavities can be combined to give a broad category of frequency-dependent rotation angles. Adopting their formulas [cf. Eqs. (A8)–(A14)] into our context, we found that, in order to realize an *additional* squeezing angle $\lambda(\Omega)$ with the form of

$$\tan\lambda(\Omega) = \frac{\sum_{k=0}^{n} B_k \Omega^{2k}}{\sum_{k=0}^{n} A_k \Omega^{2k}}, \quad |A_n + iB_n| > 0, \tag{21}$$

we first need to obtain an initial frequency-independent squeezed state with

$$\lambda_0 = \arg(A_n - iB_n), \tag{22}$$

and then filter this squeezed light with n filters whose complex resonant frequencies differ from ω_0 by $\Omega_J^{\rm res} \equiv -\delta_J \xi_J - i\delta_J$, $J = 1,2,\ldots,n$, with $\{\pm\Omega_J^{\rm res}\}$ being the $2n$ roots of the *characteristic equation*

$$\sum_{k=0}^{n} (A_k - iB_k)\Omega^{2k} = 0. \tag{23}$$

(Note that $\{\Omega_J^{\rm res}\}$ are the n roots with the appropriate sign of the imaginary part, in our case negative.)

Suppose the readout quadrature ζ is frequency independent, then from the ideal input-output relation of GEO 600 we see that the desired λ from Eq. (16) is indeed of the form of Eq. (21) when $\Omega L/c$ is expanded to the leading order [42]. Two filter cavities are necessary for the generic case. However, as we look at the low-power limit, only one such filter is necessary. In this case, the input-output relation rotates the input quadratures into the output quadratures following the same law as for a detuned cavity. Naturally, as we go through Eqs. (22) and (23), we find that the required initial additional squeezing angle is

$$\lambda_0 = \zeta - \pi/2, \tag{24}$$

which puts the minor axis of the noise ellipse onto the ζ quadrature, while the required cavity has resonant frequency

$$\Omega^{\rm filter\ res} = \frac{\phi_{\rm FP} c}{L_{\rm FP}} - i\frac{c\tau_{\rm FP}^2}{4L_{\rm FP}}, \tag{25}$$

which is just ''opposite'' to the signal-recycling resonant frequency

$$\Omega^{\rm SR\ res} \equiv \omega^{\rm SR} - i\gamma^{\rm SR} = -\frac{\phi c}{L} - i\frac{c\tau^2}{4L}, \tag{26}$$

and cancels the rotation induced by signal recycling.

For full-power GEO 600 interferometers, the initial additional squeezing angle is still given by Eq. (24), while the frequency-dependent part requires two cavities determined by the following characteristic equation:

$$\Omega^2(\Omega + \omega^{\rm SR} + i\gamma^{\rm SR})(\Omega - \omega^{\rm SR} - i\gamma^{\rm SR}) - \frac{10P\omega_0}{mLc}[\omega^{\rm SR} + 2e^{i\zeta}\sin(\zeta)\gamma^{\rm SR}] = 0. \tag{27}$$

It is straightforward to solve for the four roots (in two pairs) of the characteristic equations. The corresponding transmissivity τ of the input mirror and the detuning ϕ of the filter cavity can be derived from these roots by virtue of Eq. (25).

IV. SIGNAL RECYCLING, SQUEEZED-LIGHT INPUT, AND VARIATIONAL OUTPUT

As shown by Kimble *et al.* [14], the quantum noise spectral density of a conventional interferometer without signal recycling can benefit simultaneously from both frequency-dependent squeezed-light input and frequency-dependent homodyne readout. In this section we investigate the optical-spring signal-recycled interferometer with corresponding additional input and output optics. We start from the result of the previous section and vary the angle ζ of homodyne detection.

Figure 4 shows an array of eight noise spectral density curves of the output quadrature detection angle ζ varied from 0 to 1.4 in equidistant steps. Note that for all eight curves plotted here (thin lines and bold dashed line) the output quadrature detection angle is still frequency independent, and the input vacuum at the dark port is optimally squeezed with squeezing parameter $r = 1$. Obviously, the array is bounded from below, as indicated by the bold curve. This boundary corresponds to the optimized quantum noise spectral density of the signal-recycled interferometer. Comparing the bold dashed curve with the optimized noise spectral density, one can see that the variational output provides a further improvement of the interferometer's performance which is

mainly an increased bandwidth of the sub-SQL sensitivity. At some frequencies the noise is reduced by a factor of 10. We emphasize that the optimized noise spectrum presented cannot be further improved for this interferometer topology without increasing the squeezing parameter r of the input vacuum. Obviously, our results are also significant without any squeezing of the input vacuum. The plots in Fig. 4 are not altered except for a shift upward by a factor of e^r.

In the final part of this section we give an analytical expression for the lower boundary starting from Eq. (17). S_h^{SI} has to be minimized with respect to the detection angle ζ. One method to find the minimum noise is to determine analytically the minimum of the function $S_h^{\mathrm{SI}}(\zeta)$. Then, a lengthy but straightforward calculation leads to a conditional equation for the optimized detection angle ζ_{opt} of the following form [43]:

$$(\cos\zeta_{\mathrm{opt}}\ \sin\zeta_{\mathrm{opt}})\begin{pmatrix} Q_{11} & Q_{12} \\ Q_{12} & Q_{22}\end{pmatrix}\begin{pmatrix}\cos\zeta_{\mathrm{opt}} \\ \sin\zeta_{\mathrm{opt}}\end{pmatrix}=0. \qquad (28)$$

Representing a general SR interferometer, the coefficients of the symmetric quadric **Q** are complex (and complex-valued) functions of the interferometer parameters $(\mathcal{K},\Phi,\ldots)$ that determine the input-output relation Eq. (2). It is more convenient to express them in terms of the elements of the two symmetrized matrices $\mathcal{S}=\langle \mathbf{s}\,\mathbf{s}^{\dagger}\rangle_{\mathrm{sym}}$, $\mathcal{T}=\langle \mathbf{T}\,\mathbf{T}^{\dagger}\rangle_{\mathrm{sym}}$:

$$\begin{aligned} Q_{11}&=\mathcal{S}_{11}(\mathcal{T}_{12}+\mathcal{T}_{21})-\mathcal{T}_{11}(\mathcal{S}_{12}+\mathcal{S}_{21}),\\ Q_{12}&=\mathcal{S}_{11}\mathcal{T}_{22}-\mathcal{T}_{11}\mathcal{S}_{22}, \qquad (29)\\ Q_{22}&=\mathcal{T}_{22}(\mathcal{S}_{12}+\mathcal{S}_{21})-\mathcal{S}_{22}(\mathcal{T}_{12}+\mathcal{T}_{21}).\end{aligned}$$

In general, Eq. (28) has two solutions corresponding to a local minimum and a local maximum of the noise density:

$$\zeta_{\pm}=-\operatorname{arccot}\left[\frac{1}{Q_{11}}(\pm\sqrt{-\det\mathbf{Q}}+Q_{12})\right]. \qquad (30)$$

The minimum of the noise spectral density is given by inserting $\zeta_{\mathrm{opt}}=\zeta_{-}$ into Eq. (17). The optimized detection angle ζ_{opt} is shown in Fig. 5 together with the optimized squeezing angle λ_{opt} of the input field which depends on ζ_{opt} according to Eq. (16). The well-behaved forms of both curves suggest that the filtering of the input and output light is experimentally accomplishable. However, when applying a specific set of interferometer parameters, one first has to investigate if an expansion in the form of Eq. (21) yields an expression that represents a manageable number of filter cavities.

V. CONCLUSION

We have shown that the quantum-noise limited sensitivity of signal-recycled interferometers, like GEO 600 or Advanced LIGO, can be improved by additional input and output optics. Although an optical-spring signal-recycled interferometer ponderomotively generates squeezed light and can already beat the standard quantum limit, our results show that squeezed-light input is compatible, leading to a quantum-noise reduction by the squeezing factor e^{-2r} (in power). Variational-output optics has been proven to provide an additional benefit to the quantum-noise limited sensitivity of signal-recycled interferometers. Our work augments the results by Buonanno and Chen [8,9,12,13] and by Kimble *et al.* [14] and synthesizes their investigations.

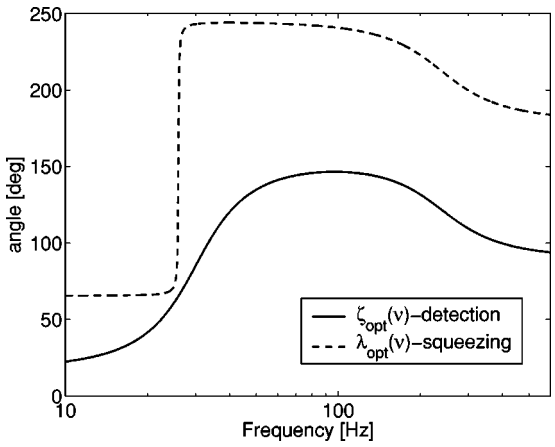

FIG. 5. The optimized detection angle ζ_{opt} is determined by Eq. (30). The optimized squeezing angle λ_{opt} of the input field depends on ζ_{opt} by virtue of Eq. (16).

We have provided fully optimized homodyning and squeezing angles, expressible in analytical formulas, although they are probably not always easily achievable with the technique proposed by Kimble *et al.*, which used detuned FP cavities as optical filters. However, in the special (suboptimal) case with frequency-independent homodyning angle but frequency-dependent input squeezing angle, we found the optimal (frequency-dependent) input squeezing angle to be achievable by applying two successive filters on frequency-independent squeezed light. We did not analyze the effect of optical losses, but as pointed out by Kimble *et al.* the frequency-dependent input-squeezing technique is less susceptible to optical losses than the variational readout and squeezed-variational schemes. A thorough study of optical losses will be published in a separate paper [34].

ACKNOWLEDGMENTS

We thank A. Freise, H. Lück, G. Heinzel, and B. Willke for many discussions providing us with valuable insight into signal-recycled interferometers. We also acknowledge N. Grosse and A. Rüdiger for their invaluable suggestions that contributed to the form and clarity of this paper. The research of Y.C. is supported by the National Science Foundation grant PHY-0099568 and by the David and Barbara Groce Fund at the San Diego Foundation. Y.C. thanks the Albert-Einstein-Institut in Hannover for support during his visit. Y.C. also thanks Alessandra Buonanno for collaboration in numerous earlier works, from which his contributions to this paper have benefited.

[1] K. S. Thorne, in *300 Years of Gravitation*, edited by S. W. Hawking and W. Isreal (Cambridge University Press, Cambridge, England, 1987), pp. 330–458.
[2] B. Willke *et al.*, Class. Quantum Grav. **19**, 1377 (2002).
[3] A. Abramovici *et al.*, Science **256**, 325 (1992).
[4] M. Ando *et al.*, Phys. Rev. Lett. **86**, 3950 (2001).
[5] B. Caron *et al.*, Class. Quantum Grav. **14**, 1461 (1997).
[6] R. W. P. Drever *et al.*, in *Quantum Optics, Experimental Gravitation, and Measurement Theory*, edited by P. Meystre and M. O. Scully (Plenum, New York, 1983), pp. 503–514.
[7] B. J. Meers, Phys. Rev. D **38**, 2317 (1988).
[8] A. Buonanno and Y. Chen, Class. Quantum Grav. **18**, L95 (2001).
[9] A. Buonanno and Y. Chen, Phys. Rev. D **64**, 042006 (2001).
[10] K. A. Strain and B. J. Meers, Phys. Rev. Lett. **66**, 1391 (1991).
[11] E. Gustafson, D. Shoemaker, K. Strain, and R. Weiss, ''LSC White paper on Detector Research and Development,'' LIGO Document No. T990080-00-D, Caltech/MIT, 1999. See also www.ligo.caltech.edu/ligo2/. Please note that this reference did not take into account the correct quantum-noise calculations that were later done by Buonanno and Chen.
[12] A. Buonanno and Y. Chen, Phys. Rev. D **65**, 042001 (2002).
[13] A. Buonanno and Y. Chen, Phys. Rev. D **67**, 062002 (2003).
[14] H. J. Kimble, Y. Levin, A. B. Matsko, K. S. Thorne, and S. P. Vyatchanin, Phys. Rev. D **65**, 022002 (2002).
[15] C. M. Caves, Phys. Rev. D **23**, 1693 (1981).
[16] W. G. Unruh, in *Quantum Optics, Experimental Gravitation, and Measurement Theory* [6], p. 647.
[17] J. Geabanacloche and G. Leuchs, J. Mod. Opt. **34**, 793 (1987).
[18] M. T. Jaekel and S. Reynaud, Europhys. Lett. **13**, 301 (1990).
[19] A. F. Pace, M. J. Collett, and D. F. Walls, Phys. Rev. A **47**, 3173 (1993).
[20] S. P. Vyatchanin and A. B. Matsko, JETP **77**, 218 (1993).
[21] S. P. Vyatchanin and A. B. Matsko, Phys. Lett. A **203**, 269 (1995).
[22] S. P. Vyatchanin and A. B. Matsko, JETP **82**, 1007 (1996).
[23] S. P. Vyatchanin and A. B. Matsko, JETP **83**, 690 (1996).
[24] S. P. Vyatchanin, Phys. Lett. A **239**, 201 (1998).
[25] C. M. Caves and B. L. Schumaker, Phys. Rev. A **31**, 3068 (1985); B. L. Schumaker and C. M. Caves, *ibid.* **31**, 3093 (1985).
[26] J. Mizuno, K. A. Strain, P. G. Nelson, J. M. Chen, R. Schilling, A. Rüdiger, W. Winkler, and K. Danzmann, Phys. Lett. A **175**, 273 (1993).
[27] J. Mizuno, ''Comparison of Optical Configurations for Laser-Interferometric Gravitational-Wave Detectors,'' Ph.D. thesis, Universität Hannover and Max-Planck-Institut für Quantenoptik, Garching, 1995, MPQ Report No. 203, 1995.
[28] G. Heinzel, ''Advanced Optical Techniques for Laser-Interferometric Gravitational-Wave Detectors,'' Ph.D. thesis, Universität Hannover and Max-Planck-Institut für Quantenoptik, Garching, 1999, MPQ Report No. 243, 1999.
[29] G. Heinzel, J. Mizuno, R. Schilling, A. Rüdiger, W. Winkler, and K. Danzmann, Phys. Lett. A **217**, 305 (1996).
[30] G. Heinzel, K. A Strain, J. Mizuno, K. D. Skeldon, B. Willke, W. Winkler, R. Schilling, A. Rüdiger, and K. Danzmann, Phys. Rev. Lett. **81**, 5493 (1998).
[31] A. Freise, G. Heinzel, K. A Strain, J. Mizuno, K. D. Skeldon, H. Lück, B. Willke, R. Schilling, A. Rüdiger, W. Winkler, and K. Danzmann, Phys. Lett. A **277**, 135 (2000).
[32] J. Harms, ''Quantum Noise in the Laser-Interferometer Gravitational-Wave Detector GEO600,'' Diploma thesis, Universität Hannover, 2002, available at http://www.geo600.uni-hannover.de/personal/harms.html
[33] V. B. Braginsky and A. B. Manukin, Zh. Éksp. Teor. Fiz. **52**, 987 (1967) [Sov. Phys. JETP **25**, 653 (1967)].
[34] J. Harms *et al.* (in preparation).
[35] V. B. Braginsky, M. L. Gorodetsky, F. Ya. Khalili, A. B. Matsko, K. S. Thorne, and S. P. Vyatchanin, Phys. Rev. D **67**, 082001 (2003).
[36] V. Chickarmane and S. V. Dhurandhar, Phys. Rev. A **54**, 786 (1996).
[37] V. Chickarmane, S. V. Dhurandhar, T. C. Ralph, M. Gray, H.-A. Bachor, and D. E. McClelland, Phys. Rev. A **57**, 3898 (1998).
[38] D. F. Walls and G. J. Milburn, *Quantum Optics* (Springer, Berlin, 1995).
[39] G. Breitenbach, F. Illuminati, S. Schiller, and J. Mlynek, Europhys. Lett. **44**, 192 (1998).
[40] P. Purdue and Y. Chen, Phys. Rev. D **66**, 122004 (2002).
[41] The coupling constant for the Advanced LIGO configuration can be expressed in another form which highlights the distinguishing properties as well as the similarities even more clearly:

$$\mathcal{K}_{\mathrm{LIGO}}=\frac{32P\omega_0}{mc^2\Omega^2}\left|1-\sqrt{1-\tau_{\mathrm{arm}}^2}e^{2i\Omega L/c}\right|^{-2}.$$

[42] Note that one has to take $\Omega L/c\sim T_{\mathrm{SR}}\sim\phi\sim\mathcal{K}$ in order to get a meaningful expansion.
[43] A similar analytic expression has also been obtained independently by Buonanno and Chen, but remained unpublished.